Materials Advances

ROYAL SOCIETY OF CHEMISTRY

COMMUNICATION

View Article Online
View Journal | View Issue



Cite this: *Mater. Adv.*, 2026, 7, 2012

Received 14th November 2025,
Accepted 22nd December 2025

DOI: 10.1039/d5ma01328c

rsc.li/materials-advances

# A 24/7 perovskite catalyst through oxygen vacancy engineering for the rapid catalytic degradation of azo dyes under dark and ambient light conditions

Suruthi Rajendran,† Dhakshnamoorthi Harikaran † and Vijayaraghavan R *

**Oxygen vacancies are introduced into the perovskite $BaSnO_3$ through the controlled substitution of $Sn^{4+}$ by $Cu^{2+}$, and their presence is confirmed by X-ray photoelectron spectroscopy and electron spin resonance. These electron-rich vacancies actively generate reactive oxygen species (ROS) in the dark (in the absence of light) and under ambient light conditions in an aqueous medium, as verified through scavenger studies and terephthalic acid and nitroblue tetrazolium assays. The role of oxygen vacancies in ROS formation is further validated by comparative substitution of $Cu^{2+}$ and $Nb^{5+}$ at the Sn site. Notably, $BaSn_{1.8}Cu_{0.2}O_3$ exhibits ultrafast catalytic degradation of four different toxic azo dyes, achieving more than 90% degradation within 20–60 minutes under both dark and ambient light conditions, surpassing many reported catalysts. In particular, amaranth dye showed 91.1% degradation within 20 minutes, with a high rate constant of $14.5 \times 10^{-2}$ $min^{-1}$ under dark conditions. TOC removal efficiencies of 43.9% and 59.6% for methyl orange and acid orange II, respectively, confirm the substantial mineralisation of the dyes to $CO_2$ and $H_2O$. HRMS analysis enables the identification of intermediates and the elucidation of possible degradation pathways, while ECOSAR toxicity predictions indicate that the degradation process reduces the ecotoxicity of the products. Overall, these results highlight the exceptional potential of this system for round-the-clock environmental remediation.**

## Introduction

Perovskites are an important family of oxides that have been studied extensively for their properties and applications.[1] These are versatile materials with multiple functional properties, useful in applications such as photocatalysis, superconductors, ferroelectric devices, thermoelectric generators, and magnetic materials. In particular, photocatalysis is an advanced oxidation process (AOP) that offers an efficient and cost-effective method for generating reactive oxygen species (ROS).[2] In this process, semiconductors, upon excitation with light, create electrons ($e^-$) and holes ($h^+$), which drive the photocatalytic redox process.[3] Most perovskites exhibit strong photon absorption due to their wide band gaps, while their structural, compositional, and stoichiometric tunability further enhances their potential for photocatalysis.[4] Well-known photocatalysts, such as $TiO_2$, ZnO, and $BiVO_4$, require light energy in the UV or visible range for activation. From a practical perspective, these processes require high photon usage, leading to increased energy consumption, financial costs, and the need for specialized catalysts. To address these challenges, dark (absence-of-light) catalysis has been explored. Dark catalysts offer the advantage of functioning without photons or external energy, without chemicals, making them highly attractive in AOP-based catalysis.[5] There is a need to develop catalysts that produce ROS in the dark, enabling AOP to be carried out in the dark and extended to ambient light.

Oxygen vacancies (OVs) are ubiquitous point defects that occur when an oxygen atom is removed from the lattice oxygen ($O_2$) of metal oxides under specific external conditions. OVs are among the most commonly studied anionic vacancies owing to their ease of formation.[6] Recent studies have confirmed that oxygen vacancy engineering effectively enhances catalytic activity.[7] Defects can arise from aliovalent doping, high-temperature treatment, or exposure to reducing environments.[8] In perovskite oxides, doping with iso- and aliovalent ions induces interstitial strain and structural defects, modifying the electronic structure and improving the catalytic properties.[9] In dark catalysis, the oxygen vacancies in perovskites introduce excess electrons that interact with dissolved oxygen molecules to generate ROS. Earlier studies on the perovskite systems $CaFe_{1-x}Ni_xO_{3-\delta}$, $La_{1-x}Sr_xCoO_{3-\delta}$, $LaNiO_{3-\delta}$, and $SrFeO_{3-\delta}$ highlight the role of oxygen vacancies in dark catalytic degradation of organic pollutants.[10] Although these catalysts are reported to work in the dark, they have not been studied under ambient light. Since AOPs conventionally require light to drive ROS production, understanding Ovs' mediated pathways in both dark and ambient light conditions is essential for achieving round-

*Department of Chemistry, School of Advanced Sciences, Vellore Institute of Technology, Vellore, 632 014, India. E-mail: rvijayaraghavan@vit.ac.in*
† These authors contributed equally to this work.

the-clock (24/7) catalytic activity. Unlike Fenton or afterglow-based processes, which require additional reagents (*e.g.*, $H_2O_2$, $Fe^{2+}$) or external energy,[11] OVs-driven dark catalysis provides a sustainable and self-sufficient approach for environmental remediation as day–night catalysts.

Perovskite $ASnO_3$ (A = Ca, Sr, Ba) comprises corner-sharing $SnO_6$ octahedra, with the Goldschmidt tolerance factor determining structural stability and phase. $BaSnO_3$ ($t \approx 1.02$) forms a stable cubic phase, while $SrSnO_3$ and $CaSnO_3$ adopt orthorhombic structures.[12] A- and B-site substitutions further tune crystal symmetry and electronic structure. Lower-valent cation substitution at the B site creates surface oxygen vacancies, which act as reactive centres in catalytic reactions.[13] Azo dyes (–N═N–), extensively used across the food, textile, leather, pharmaceutical, and cosmetic industries for their solubility and stability, pose serious environmental and health risks due to their persistence and non-biodegradability, highlighting the need for efficient advanced oxidation processes to remove them from industrial effluents.[14]

In this work, we report the incorporation of Cu as a B-site dopant in $BaSnO_3$. The introduction of Cu induces oxygen vacancies within the $BaSn_{1-x}Cu_xO_3$ lattice, which play a pivotal role in catalytic activity. Surface oxygen vacancies serve as active sites that facilitate ROS generation, enabling the degradation of azo dyes even in dark conditions. Notably, the catalyst remains active under ambient conditions, ensuring continuous performance (24/7). $BaSn_{1-x}Cu_xO_3$ exhibits superior catalytic efficiency toward the degradation of representative azo dyes, including methyl orange, acid orange II, Congo red, and amaranth. Its performance is much superior to all reported catalysts. This is the first example of an oxide system in which oxygen vacancies have been systematically varied and correlated to their activity under dark and ambient light. This opens up many possibilities in different families of oxides, which could be explored as round-the-clock catalysts.

Cu-doped $BaSnO_3$ material was synthesised by the solid-state method described in the materials and catalytic experiment method as given in Text S1. The above method introduces vacancies under heat-treatment conditions. The instrumentation details are summarised in Text S2. The XRD patterns of $BaSnO_3$ [BS] and $BaSn_{1-x}Cu_xO_3$ ($x$ = 0.05 [BS1], 0.1 [BS2], 0.15 [BS3] & 0.2 [BS4]) are shown in Fig. S1. Clearly, the diffraction peaks are matched with the corresponding JCPDS card (00-015-0780) of $BaSnO_3$. The lattice parameters of $BaSn_{1-x}Cu_xO_3$ are found to be in the range 3.73 to 4.12 Å. XPS spectra were used to identify the chemical states of the metals and to quantify the oxygen vacancies in $BaSn_{1-x}Cu_xO_3$ (Fig. 1a). The XPS spectra of O 1s show the three types of peaks: lattice oxygen ($O_L$), vacancy oxygen ($O_v$), and adsorbed or hydroxyl oxygen ($O_H$). The areas under the curve of the three characteristic peaks are tabulated in Table S1. The peak at 531.6 eV reveals oxygen vacancies of BS and BS4 within the lattice. The deconvolution peaks indicate that Ov is formed in the high-temperature-treated products, and $O_V$ increases when an aliovalent ion of $Cu^{2+}$ is doped at the Sn site in the stannate system. Overall, the $O_v$ concentration increases from 25.7% to 39.2% across BS to BS4 catalysts,

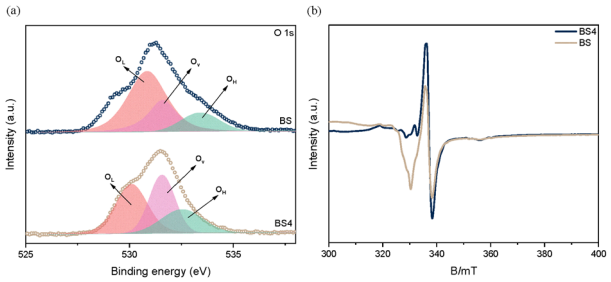


Fig. 1 (a) XPS O 1s and (b) solid ESR spectra of BS and BS4.

confirming the successful synthesis of oxygen-vacancy-enriched BS4. The other Ba 3d, Sn 3d, and Cu 2p deconvoluted spectra are shown in Fig. S2 and Text S3. Furthermore, the oxygen vacancy is confirmed by electron spin resonance (ESR) spectra (Fig. 1b). The ESR signal intensity of BS4 is higher than that of BS, indicating the greater concentration of surface oxygen-vacancy electrons in the Cu-doped stannate system. The field emission scanning electron microscopy (FESEM) images reveal that the pure BS exhibits an irregular morphology, whereas BS4 forms a cuboidal structure. The average particle sizes are found to be 245 and 142 nm for BS and BS4, respectively (Fig. S3). Elemental mapping indicates a homogeneous distribution of Ba, Sn, Cu, and O elements throughout the BS and BS4 catalyst (Fig. S4).

The catalytic degradation of azo dyes using BS and BS1–BS4 compositions was evaluated using a UV-vis spectrophotometer. Various azo dyes, including methyl orange (MO), Congo red (CR), acid orange II (AO II), and amaranth (AM), were studied, with optimization of parameters such as catalyst dosage and scavenger effects. Dark degradation results for BS and BS1–BS4 are presented in Fig. 2a. The degradation is confirmed by the decrease of absorbance at the maximum wavelength of the dyes. The UV-vis spectrum of the catalyst–dye mixture, which was kept undisturbed for 60 minutes without any stirring,

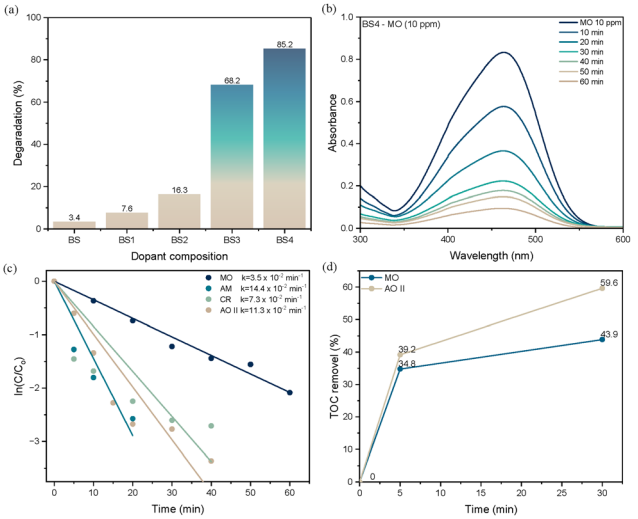


Fig. 2 (a) Dark degradation using BS, BS1, BS2, BS3, and BS4, (b) degradation curves, (c) the kinetics of various dyes (MO, AM, CR, and AO II) under dark conditions, and (d) TOC analysis of MO and AO II.

exhibited no decrease in absorbance. This suggests that without stirring, the catalyst shows negligible interaction with the dye, and no observable adsorption or degradation occurs (Fig. S5). After 60 minutes of stirring, the degradation efficiencies of MO (10 ppm) are 3.4%, 7.6%, 16.3%, 68.2%, and 87.6% for BS, BS1, BS2, BS3, and BS4, respectively. The enhanced performance of BS4 can be attributed to its higher density of oxygen vacancies, which promotes more efficient dye degradation even under dark conditions. Consequently, BS4 was selected for further investigations, and its degradation profile is presented in Fig. 2b and Fig. S5. The rate constant of BS4 for MO degradation is determined to be $3.5 \times 10^{-2}$ $min^{-1}$, which is significantly higher than that of previously reported catalysts (Fig. 2c). Furthermore, the catalytic proficiency of BS4 was assessed against a series of structurally distinct azo dyes, including CR, OR II, and AM (Fig. 2c), with the associated kinetic values and degradation efficiencies summarized in Table 1.

The catalyst dosage plays a crucial role in catalytic efficiency by influencing the number of available active sites. Experiments conducted with catalyst doses of 25, 50, and 100 mg for MO degradation in the dark are shown in Table 1 and Fig. S5. Based on these results, 100 mg was identified as the optimal catalyst dosage for degradation. A similar experimental procedure was employed under ambient light conditions, in which the catalyst retained high efficiency (Table 1), leading to effective degradation of all azo dyes (Fig. S6). The catalytic performance demonstrates a remarkably rapid degradation of azo dyes under dark conditions, achieving near-complete degradation within 20 minutes for AM dye with a high rate constant of $14.5 \times 10^{-2}$ $min^{-1}$. The BS4 catalyst demonstrates high performance, achieving rapid and high degradation of azo dyes, surpassing many reported catalysts in the literature that typically require longer reaction times (Table S2). Its high effectiveness is particularly notable under both dark and ambient-light conditions for the selected azo dyes.

Total organic carbon (TOC) was analysed to estimate residual organic compounds. It is found that the TOC removal percentage of BS4 is 43.9% and 59.6% for MO and AO II, respectively, indicating substantial conversion of the pollutants into $CO_2$ and $H_2O$ (Fig. 2d). These results clearly demonstrate that BS4 can effectively mineralize azo dyes even under dark conditions, highlighting its strong potential for practical wastewater treatment applications. High-resolution mass spectrometry (HRMS) analysis was employed to identify the degradation products and intermediates of MO and AO II, as shown in Fig. S7. During the degradation process, the intermediate products were qualitatively identified and characterized. MO degradation proceeds through three distinct pathways involving 11 intermediates, whereas AO II degradation follows three pathways involving 10 intermediates. These results collectively reveal the possible degradation mechanisms for both dyes. The proposed mechanisms and their explanations are presented in Fig. S8 and Text S4. Furthermore, the ECOSAR software model assessed the acute and chronic toxicity of degradation intermediates (Tables S3 and S4), identifying some toxic intermediates that eventually mineralise into non-toxic products with extended reaction times. Overall, the results demonstrate that this catalyst effectively facilitates the decontamination of azo dyes under dark conditions.

The specific surface area of BS4 was 0.61 $m^2$ $g^{-1}$, with a pore size distribution centred at 60.7 nm (Fig. S9). These results indicate that the material possesses a low surface area and minor porosity, providing less capacity for effective adsorption of dye molecules.[5] The scavenger study was conducted to identify the reactive oxygen species involved in the dark-catalysed reaction of BS4, using trapping experiments with *p*-benzoquinone (*p*-BQ), isopropyl alcohol (IPA), silver nitrate ($AgNO_3$) and sodium pyruvate (SP) to target superoxide radicals ($^{\bullet}O_2^-$), hydroxyl radicals ($^{\bullet}OH$), electrons, and hydrogen peroxide, respectively. The degradation experiments revealed that methyl orange (MO) degradation was significantly inhibited by electron scavenging with $AgNO_3$, with removal efficiency dropping from 87.6% to 12.5% (Fig. 3). Similarly, the use of *p*-BQ, IPA, and SP reduced the degradation efficiency to 29.0%, 63.5%, and 60.6%, respectively. The scavenger findings indicate that electrons play the dominant role in the degradation of MO, followed by superoxide radicals. The generation of reactive oxygen species (ROS) was examined using terephthalic acid for hydroxyl radicals ($^{\bullet}OH$) and nitro blue tetrazolium (NBT) for superoxide radicals ($^{\bullet}O_2^-$). The analysis revealed that the BS catalyst did not produce detectable ROS, whereas the BS4 catalyst efficiently generated both $^{\bullet}OH$ and $^{\bullet}O_2^-$ even in the absence of photon irradiation (Fig. 3 and Fig. S10).

To verify the role of OVs in catalytic activity, we introduced higher-valent cation doping as a strategy to suppress OV formation. Specifically, $Nb^{5+}$ ($x$ = 0.2) was substituted for Sn, leading to a reduction in surface oxygen-vacancy defects. The Nb-doped $BaSnO_3$ samples were synthesized using the same solid-state route and evaluated for dark catalytic activity. The degradation efficiencies for MO and AO II were found to be only 8.3% and 18.3%, respectively, confirming the limited activity (Fig. S11). This indicates that ROS generation in the dark is primarily governed by OV-mediated processes. In this study, $Cu^{2+}$ and $Nb^{5+}$ were carefully chosen as dopants to systematically tune the oxygen vacancy concentration. Interestingly, the $BaSn_{1-x}Cu_xO_3$ series exhibits OVs tuned by composition, with $x$ = 0.2 showing the highest catalytic activity under both

Table 1 Influence of catalyst dosage and dye variation on the degradation and kinetics of BS4

| Condition (BS4) | Catalyst amount (mg) | Dye (10 ppm) | % degradation (min) | Kinetics ($\times 10^{-2}$ $min^{-1}$) |
|---|---|---|---|---|
| Catalyst dosage variation – dark | 25 | MO | 11.1 (30) | 0.7 |
| | 50 | | 55.5 (60) | 1.3 |
| | 100 | | 85.4 (60) | 3.5 |
| Various dyes – dark | 100 | AM | 91.1 (20) | 14.4 |
| | | CR | 97.2 (40) | 7.3 |
| | | AO II | 93.2 (40) | 11.3 |
| Various dyes – ambient | 100 | MO | 86.7 (70) | 3.2 |
| | | AM | 93.2 (20) | 14.5 |
| | | CR | 97.2 (40) | 7.2 |
| | | AO II | 93.4 (40) | 11.3 |

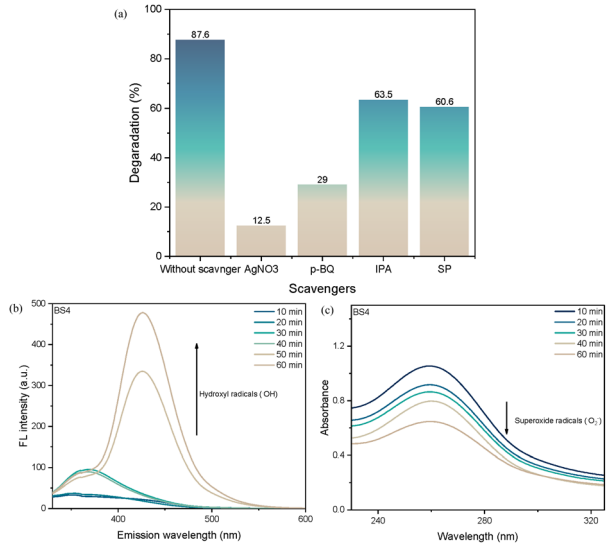


Fig. 3 (a) Scavenger studies, (b) fluorescence spectral analysis, and (c) degradation studies of NBT using BS4.

dark and ambient light conditions. In contrast, $BaSn_{1.8}Nb_{0.2}O_3$, which contains the least oxygen vacancies, displayed negligible catalytic performance.

Lakshmi Prasanna *et al.* reported a mechanism for the generation of ROS in the dark by nano-ZnO for antibacterial applications.[15] Based on this mechanism, the oxygen vacancies in BS4 can generate ROS even in the absence of photons, which supports our confirmation of the mechanism in azo dye degradation (Fig. 4). It indicates that oxygen vacancies possess excess electrons (ESR). These electrons react with dissolved oxygen to form superoxide radicals. The superoxide radicals then react with water to produce hydroperoxyl radicals (eqn (1)–(2)). The hydroperoxyl radicals combine to form $H_2O_2$, which further reacts with superoxide radicals to generate hydroxyl radicals and hydroxyl ions (eqn (3)–(4)). The reactive oxygen species (ROS) generated through this process facilitate the degradation of toxic dye molecules into harmless end products without the need for photon irradiation. The degradation under ambient light proceeds *via* an exact mechanism. This approach offers a promising strategy for contaminants removal from water under dark conditions, presenting significant potential for energy-efficient wastewater treatment.

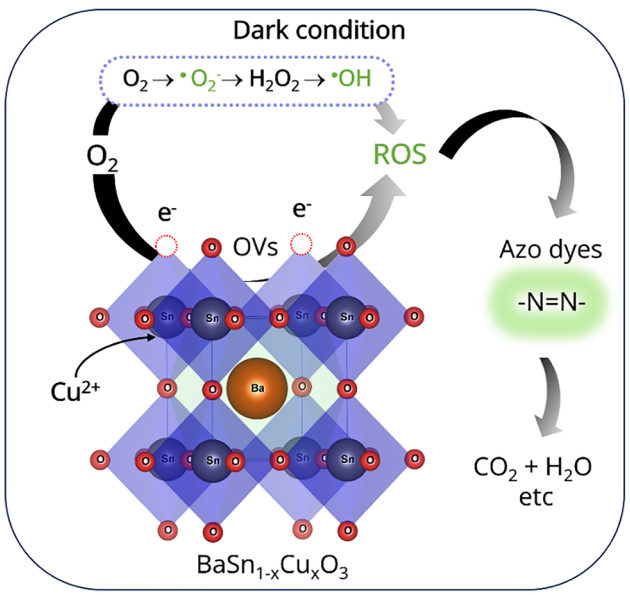


Fig. 4 The mechanism of dark degradation using $BaCu_{0.2}Sn_{0.8}O_3$.

$$O_2 + e^- \rightarrow {}^{\bullet}O_2^- \quad (1)$$

$$H_2O + {}^{\bullet}O_2^- \rightarrow {}^{\bullet}HO_2 + OH^- \quad (2)$$

$$2\,{}^{\bullet}HO_2 \rightarrow H_2O_2 + O_2 \quad (3)$$

$$H_2O_2 + {}^{\bullet}O_2^- \rightarrow O_2 + OH^- + {}^{\bullet}OH \quad (4)$$

The reusability of the catalyst is an essential parameter for practical application, and a study was conducted on MO, AO II, CR, and AM over three cycles. For AM and CR, the degradation efficiency remained above 85% after three successive runs, indicating good structural stability and reusability. In the case of AO II and MO, a gradual decrease in degradation efficiency was observed, dropping from $>90\%$ in the first cycle to $\sim 50\%$ in the third cycle, which may be due to the blocking of active sites. These findings demonstrate the catalyst's practical reusability in the dark-catalysed degradation process. The material's stability was analysed using PXRD. Fig. S12 shows that the XRD patterns for BS4 are similar before and after the reaction. This confirms the good stability and reusability of the dark catalyst.

## Conclusions

In summary, we have developed an oxygen-vacancy-engineered Cu-doped $BaSnO_3$ system for efficient dark and ambient light catalytic degradation of azo dyes. Oxygen vacancies were introduced by Cu-doping $BaSnO_3$ up to 20% *via* high-temperature solid-state synthesis. These vacancies, possessing excess electrons, react with dissolved oxygen to generate reactive oxygen species (ROS) even in the absence of light and under ambient light conditions. In particular, $BaSn_{0.8}Cu_{0.2}O_3$ exhibits the ultrafast catalytic degradation of four different toxic azo dyes under both dark and ambient light conditions, demonstrating its exceptional potential for round-the-clock environmental remediation. The TOC removal efficiencies reached 59.6% and 43.9%, indicating that most of the AO II and MO was ultimately mineralized to $CO_2$ and $H_2O$. In addition, the possible degradation pathways, intermediates, and their toxicity were identified for AO II and MO using HRMS and the ECOSAR program. The present work opens up many possibilities involving different families of oxides as day–night catalysts for environmental remediation.

## Author contributions

R. S.: methodology, investigation, visualization, data curation, formal analysis. D. H.: methodology, investigation, visualization,

data curation, formal analysis, writing – original draft. V. R.: conceptualization, supervision, writing – review & editing, funding acquisition, project administration.

## Conflicts of interest

There are no conflicts to declare.

## Data availability

All relevant data are within the manuscript and the supplementary information (SI). Supplementary information is available. See DOI: https://doi.org/10.1039/d5ma01328c.

## Acknowledgements

This work was financially supported by Vellore Institute of Technology (VIT), Vellore under the Faculty Seed Grant (RGEMS) (Sanction Order No.: SG20250013).

## Notes and references

1 S. J. J. Kay, A. Thirumurugan, S. Gobalakrishnan and N. Chidhambaram, *Coord. Chem. Rev.*, 2025, **545**, 217020; A. Žužić, A. Ressler and J. Macan, *Ceram. Int.*, 2022, **48**, 27240–27261.

2 Y. Shang, X. Xu, B. Gao, S. Wang and X. Duan, *Chem. Soc. Rev.*, 2021, **50**, 5281–5322.

3 Y. Tang, C. H. Mak, G. Jia, K.-C. Cheng, J.-J. Kai, C.-W. Hsieh, F. Meng, W. Niu, F.-F. Li, H.-H. Shen, X. Zhu, H. M. Chen and H.-Y. Hsu, *J. Mater. Chem. A*, 2022, **10**, 12296–12316; A. Kumar, A. Kumar and V. Krishnan, *ACS Catal.*, 2020, **10**, 10253–10315.

4 H. Mai, D. Chen, Y. Tachibana, H. Suzuki, R. Abe and R. A. Caruso, *Chem. Soc. Rev.*, 2021, **50**, 13692–13729; M. Humayun, Z. Li, M. Israr, A. Khan, W. Luo, C. Wang and Z. Shao, *Chem. Rev.*, 2025, **125**, 3165–3241.

5 W. Z. Li, Z.-T. Liu, X.-S. Zhang, Y. Liu and J. Luan, *Inorg. Chem.*, 2024, **63**, 7034–7044; M. Wang, G. Tan, B. Zhang, Y. Wang, Y. Bi, Q. Yang, Y. Liu, T. Liu, Z. Wang, H. Ren, L. Lv, A. Xia, L. Yin, Q. Yuan, W. Liu and Y. Liu, *Appl. Catal., B*, 2023, **321**, 122052.

6 Z. Li, X. Mao, D. Feng, M. Li, X. Xu, Y. Luo, L. Zhuang, R. Lin, T. Zhu, F. Liang, Z. Huang, D. Liu, Z. Yan, A. Du, Z. Shao and Z. Zhu, *Nat. Commun.*, 2024, **15**, 9318.

7 S. Mo, Q. Zhang, J. Li, Y. Sun, Q. Ren, S. Zou, Q. Zhang, J. Lu, M. Fu, D. Mo, J. Wu, H. Huang and D. Ye, *Appl. Catal., B*, 2020, **264**, 118464.

8 K. Xu, J.-C. Liu, W.-W. Wang, L.-L. Zhou, C. Ma, X. Guan, F. R. Wang, J. Li, C.-J. Jia and C.-H. Yan, *Nat. Commun.*, 2024, **15**, 5751.

9 N. Liu, R. Wu, Y. Liu, Y. Liu, P. Deng, Y. Li, Y. Du, Y. Cheng, Z. Zhuang, Z. Kang and H. Li, *Inorg. Chem.*, 2023, **62**, 11990–12000.

10 S. V. Besegatto, A. da Silva, C. E. M. Campos, S. M. A. G. U. de Souza, A. A. U. de Souza and S. Y. G. González, *Appl. Catal., B*, 2021, **284**, 119747; X. Luo, C. Su, Z. Chen, L. Xu, L. Zhao, J. Zhao, R. Qiu and Z. Huang, *Sep. Purif. Technol.*, 2022, **300**, 121891; W. Zhong, T. Jiang, Y. Dang, J. He, S.-Y. Chen, C.-H. Kuo, D. Kriz, Y. Meng, A. G. Meguerdichian and S. L. Suib, *Appl. Catal., A*, 2018, **549**, 302–309; M. Y. Leiw, G. H. Guai, X. Wang, M. S. Tse, C. M. Ng and O. K. Tan, *J. Hazard. Mater.*, 2013, **260**, 1–8.

11 V. Lakshmi Prasanna and R. Vijayaraghavan, *J. Phys. Chem. C*, 2017, **121**, 18557–18563; X. Liu, X. Chen, Y. Li, B. Wu, X. Luo, S. Ouyang, S. Luo, A. A. Al Kheraif and J. Lin, *J. Mater. Chem. A*, 2019, **7**, 19173–19186.

12 S. Ramos-Terrón, A. D. Jodlowski, C. Verdugo-Escamilla, L. Camacho and G. de Miguel, *Chem. Mater.*, 2020, **32**, 4024–4037.

13 Y. Wang, R. Yang, Y. Ding, B. Zhang, H. Li, B. Bai, M. Li, Y. Cui, J. Xiao and Z.-S. Wu, *Nat. Commun.*, 2023, **14**, 1412; L. Bian, F. Cao and L. Li, *Small*, 2023, **19**, 2302700.

14 P. Barciela, A. Perez-Vazquez and M. A. Prieto, *Food Chem. Toxicol.*, 2023, **178**, 113935.

15 V. Lakshmi Prasanna and R. Vijayaraghavan, *Langmuir*, 2015, **31**, 9155–9162.